Journal of Hydrology 593 (2021) 125906

Contents lists available at ScienceDirect

Journal of Hydrology

journal homepage: www.elsevier.com/locate/jhydrol

Research papers

Propagation of soil moisture droughts in a hotspot region: Spatial pattern and temporal trajectory

Yongwei Liu [a], Yuanbo Liu [a,*], Wen Wang [b], Han Zhou [c]

[a] Key Laboratory of Watershed Geography Sciences, Nanjing Institute of Geography and Limnology, Chinese Academy of Sciences, Nanjing, China
[b] State Key Laboratory of Hydrology-Water Resources and Hydraulic Engineering, Hohai University, Nanjing, China
[c] Wuhan University of Technology, Wuhan, China

ARTICLE INFO

This manuscript was handled by Emmanouil Anagnostou, Editor-in-Chief, with the assistance of Viviana Maggioni, Associate Editor

Keywords:
Soil moisture drought
Drought cluster
Drought propagation
Southeastern Asia

ABSTRACT

Droughts evolve in space and time simultaneously, but its spatio-temporal propagation remains less explored. As one of the hotspot regions in global soil moisture (SM) drought, the Southeastern Asia supports billions of population and trillions of dollars in gross domestic product. Its high drought risk initiated a deep understanding of drought propagation in multiple dimensions for effective prevention. This study investigated the SM droughts with a merged dataset of remote sensing and land surface modeling over 1979–2016. Our results showed that 369 drought clusters and 145 drought events occurred. Spatially, severe droughts appeared mainly in southwest and northeast of the study region. Temporally, the droughts were more severe in cold season (winter and spring) than warm season (summer and autumn). In last four decades, the SM droughts alleviated in warm season but aggravated in cold season significantly, posing a challenge for drought mitigation, especially for spring crop growth vigorously. Furthermore, the drought clusters shared two predominant routes of westward and southwest. The westward route is for the droughts started in winter in south region, while the southwest route is for the droughts started in summer across the Yangtze River basin from northeast to southwest. At a drought event level, the SM drought propagated synergistically with precipitation and potential evapotranspiration (PET). Precipitation was generally the primary driver and PET the secondary, particularly for SM droughts lasting in summer and winter in south region. The intensity of PET usually enhanced in spring and summer with temperature increasing and crop growing. The findings in drought propagation provide essential spatiotemporal structure for mechanism exploration and important clues for drought prediction.

1. Introduction

Drought is a frequently occurred and widespread hydro-climatic extreme phenomenon. Some drought events usually last from months to years and even evolve into serious natural hazards (Dai, 2011), which have considerable unfavorable impacts on ecosystem, hydrology, agriculture and economy (Vicente-Serrano et al., 2012). Soil moisture (SM) governs the magnitude and variation of water and energy fluxes at land–atmosphere surface, being regarded as a key indicator in drought monitoring, in particular for agricultural drought. Understanding the spatio-temporal dynamics and evolution characteristics of SM drought is fundamental for further exploring its driving mechanisms and making accurate drought predictions, which is significant for agriculture production and water management.

Many studies have focused on drought investigation about its temporal (e.g. frequency, duration, tendency) and spatial (e.g. area, intensity, severity) characteristics. Sheffield and Wood (2008) analyzed the global and regional trends of drought over 1950–2000 using a SM based drought index and explored its underlying driving factors in further. Andreadis and Lettenmaier (2006) examined the drought trends of 20th century over the conterminous United States using a simulated data set of hydro-climatological variables, and found that droughts had become shorter and less frequent over most parts of the region. Liu et al. (2016) provided a regional view of the spatiotemporal characteristics of drought conditions across the entire Loess Plateau and identified the variability and trends of drought at different spatial and temporal scales. Zhou and Liu (2018) examined the spatial pattern of meteorological droughts in Poyang Lake basin in China and investigated the physical mechanism behind. Gocic and Trajkovic (2014) evaluated the spatio-temporal characteristics of drought in Sebia based on the standard

* Corresponding author.
E-mail addresses: ywliu@niglas.ac.cn (Y. Liu), ybliu@niglas.ac.cn (Y. Liu).

https://doi.org/10.1016/j.jhydrol.2020.125906
Received 28 June 2020; Received in revised form 23 October 2020; Accepted 14 December 2020
Available online 19 December 2020

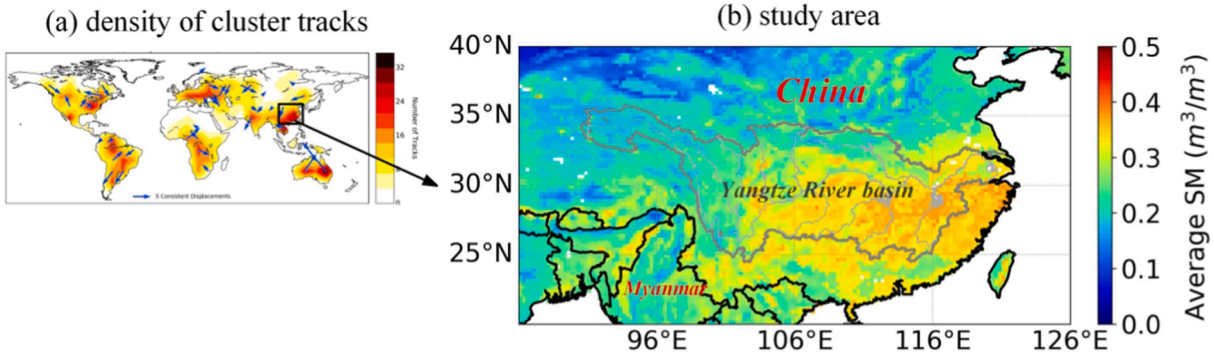

Fig. 1. (a) Density of drought cluster tracks over the globe referenced from Herrera-Estrada et al. (2017), which indicates the mobility of soil moisture droughts; (b) The study region with spatial distribution of multi-year average surface soil moisture from ESA CCI SM (v04.2) over 1979–2016. Note that Yangtze River basin (the grey line enclosed area) is marked out to highlight the location of the study region (20°N ~ 40°N, 86°E ~ 126°E). The dark gray line in Yangtze River basin represents the main streams and tributaries. The bold black line is the national boundary.

precipitation index (SPI) using the principle component analysis approach. In general, previous researches usually identify drought events from time dimension, and consequently analyze the drought characteristics from its temporal variations or spatial distributions separately, while generally neglect the space–time continuous property of the actual droughts. The lower-order subspace drought characteristic analysis tends to discard much of the spatio-temporal information, thus still insufficient in capturing the real characteristics of droughts (e.g. the spatial position changes of a drought over time, and the overall severity/duration of a drought in space–time domain) (Lloyd-Hughes, 2012).

With the improvement of the distributed hydrological model in its spatial generalization and simulation ability, in particular for the fast development of the satellite remote sensing and inversion techniques, the availability of large scale spatio-temporal continuous meteorological and hydrological variables (e.g. precipitation, soil moisture) become possible (Lievens et al., 2016; Zhang et al., 2017). It provides great advantages for time–space joint investigation of large scale droughts. To date, some reports have taken the spatio-temporal synchronous identification and characterization of droughts into consideration. Andreadis et al. (2005) introduced a clustering algorithm to consider the spatial and temporal continuous property of individual drought events, and constructed a series of severity-area-duration (SAD) curves to integrate the spatio-temporal information into drought characterization rather than reducing the drought analysis to a lower dimension. Lloyd-Hughes (2012) extended the clustering algorithm of Andreadis et al. (2005) into a longitude-latitude-time space, and demonstrated this explicit 3-dimensional (3-D) drought identification approach in the application of European drought analysis. Thereafter, Xu et al. (2015) developed a 3-D clustering method, and adopted it in a spatial and temporal variation analysis of meteorological droughts in non-arid regions of China over last four decades. The above cluster-based drought identification and the innovative SAD approaches provided a way to analyze the spatial and temporal synergistic changes of droughts, which were adopted by many later researches, e.g., Sheffield et al., 2009; Wang et al., 2011; Zhan et al., 2016; Zhai et al., 2017. These researches characterize and investigate droughts in a space–time continuous perspective, which are informative in exploring the characteristics and processes of actual droughts. Yet, most of the researches focus on spatial extent, while obscures much of the spatial–temporal evolution of the drought structure. The spatial propagation process of droughts over time is the foundation to understand the forcing on drought development, which makes it indispensable for drought mechanism exploration and drought prediction (Lloyd-Hughes, 2012). However, to our knowledge, the explicit analysis on spatio-temporal dynamic evolution of drought events is only limited to a few studies such as Herrera-Estrada et al. (2017), Guo et al. (2018), Zhou et al. (2019), and Diaz et al. (2020). What are the main places where drought frequently occurred and long lasted? What are the dynamics of the drought clusters (the spatial continuous regions under drought) during individual events? Are there predominant routes followed by drought? These issues are still subject to further investigation.

Southeastern Asia is the most populous region of the world. It contributes trillions of dollars in gross domestic product with the world's second largest economy of China. This region is also one of the world's favorable cultivation area with over 10% covered by arable agricultural land (Hannah and Max, 2013). However, Southeastern Asia is one of the most active regions of SM droughts with high drought tracking capacity over the globe (Herrera-Estrada et al., 2017). With global warming in recent years, the drought issue in various regions of Southeastern Asia is increasingly prominent. Significant dry trends were detected in large parts of south China (Zhai et al., 2017; Liu et al., 2019a). The droughts became more intense and frequent in southwest of China during the past 50 years (Yang et al., 2013; Sun et al., 2016, 2017). In recent years, Poyang Lake basin (in lower Yangtze River basin) (Liu and Wu, 2016), even the whole Yangtze River basin experienced serious drought issue (Zhou and Liu, 2018; Huang et al., 2014; Zhang et al., 2014). Moreover, it has been found that the significant dry periods become longer in Pearl River basin (located in southeastern China) from 1961 to 2007 (Fischer et al., 2011). The above serious drought conditions and scenarios bring huge damages to agriculture and ecosystem of Southeastern Asia, where many developing regions/countries are located. Considerable efforts have been dedicated to exploring the drought characteristics, even the driving mechanisms from climate perspectives (e.g. Wang et al., 2018). However, as the primacy of understanding the drought property and exploring drought mechanism, the spatio-temporal dynamic evolutionary processes and characteristics of drought in Southeastern Asia remains ambiguous up to now.

Therefore, this study focuses on the spatio-temporal dynamics and characteristics of SM droughts (directly related to agriculture drought) in Southeastern Asia, with the objectives to (i) identify the SM drought events in spatial and temporal perspective simultaneously in last four decades; (ii) investigate the spatial patterns and temporal variations of SM droughts comprehensively; (iii) explore the spatio-temporal propagation characteristic of SM droughts; and (iv) analyze the development process of individual drought events.

2. Study area and data

2.1. Study area

This study focused on the droughts in Southeastern Asia, which is one of the most active areas (i.e. hotspot regions) where SM droughts occur and propagate (see Fig. 1 (a)) over the globe. Fig. 1(b) presents the whole study area between 20°N ~ 40°N and 86°E ~ 126°E. This region is located in East Asia monsoon climate zone with the most typical

monsoon climate over the globe. The multi-year average surface SM varies between ~0.1 and ~0.45 m^3/m^3. The high SM mainly distributed in southeastern parts, including the middle and lower reaches in south bank of Yangtze River basin and the regions in Zhejiang, Fujian and Guangdong provinces in China (Fig. 1 (b)). As the largest river basin in China, Yangtze River Basin is marked out here to highlight the location of the study region.

2.2. Data

The soil moisture (SM) data used in this study is a merged multi-satellite dataset, developed in the Climate Change Initiative (CCI) project by European Space Agency (ESA) (Liu et al., 2011a, 2011b). The active and passive combined dataset (1979–2016) of ESA CCI SM (version 04.2) was utilized here, with a spatial resolution of 0.25°×0.25°, a temporal resolution of ~1 day and a soil moisture thickness of ~2 cm. For drought analysis, 1-month SM dataset was generated from temporal averaging of the daily dataset. Considering that data missing problem of ESA CCI SM dataset would degrade its performance in drought application (Yuan et al., 2015), the missing values for monthly ESA CCI SM were filled using the cumulative distribution frequency (CDF) matching approach (Reichle and Koster, 2004) based on a land surface modeling SM dataset from global land data assimilation system. Specifically, the land surface modeling SM data utilized here is the surface (0–10 cm) soil moisture from GLDASv2.0/Noah (1979–2010) and GLDASv2.1/Noah (2011–2016) after bias correction based on CDF matching approach. The data gap filling and bias correction process was detailed in Liu et al. (2019a). The data gap filling degree for the whole study region is present in Figure S1.

The precipitation, potential and actual evapotranspiration data were adopted to support the SM drought study. The monthly Global Precipitation Climatology Centre (GPCC) dataset from 1979 − 2016 with a spatial resolution of 0.25°×0.25° were utilized. The GPCC dataset was generated from the quality controlled data of 67,200 stations worldwide with the record duration of 10 years or more, of which the data quality has been verified by many researches (Cattani et al., 2016; Schneider et al., 2017). The potential evaporation rate (PET) and evapotranspiration (ET) data were extracted from GLDASv2.0/Noah (1979–2010) and GLDASv2.1/Noah (2011–2016) datasets. The biases both for PET or ET between GLDASv2.1/Noah and GLDASv2.0/Noah were corrected using the CDF rescaling method on grid scale.

3. Methodology

3.1. Drought event identification in a 3-D space–time domain

In this study, 3 monthly SM anomaly percentage index (3-SMAPI) is selected as it has been effectively applied in various long-term regional and global drought assessment (e.g. Wu et al., 2016; Liu et al., 2019a). Because this study focuses on the moderate and moderate above droughts, a threshold of −0.15 is adopted to distinguish drought cases, i.e. 3-SMAPI < -0.15 is concerned as drought condition. The drought event identification is based on a clustering method (Andreadis et al., 2005; Lloyd-Hughes, 2012), in which the space–time continuum structure of a drought is extracted from the 3-dimensional (latitude, longitude and time) array of 3-SMAPI. In specific, the identification of the spatio-temporal continuous drought events mainly includes the following two aspects.

(1) Identification of the drought cluster at each time step (month), i.e. determination of the spatial continuity of the grid pixels under drought. First, the spatial noises of each 3-SMAPI monthly map are smoothed out using a 2-D median filter. Then, the drought condition of each grid pixel over the whole region at each month from 1979 to 2016 is figured out based on the criterion of 3-SMAPI < -0.15. The dry grid pixels with spatial continuity are regarded as one individual drought cluster. Small clusters with their area less than 62,500 km^2 (i.e. ~100 grids, approximately 1.5% of the study region) are ignored in the following drought event identification procedure. This area truncation practice is to avoid the appearance of spurious long drought events due to the tenuous spatial continuity. The truncation threshold in this study is analogous to that adopted by Liu et al. (2019b) and Wang et al. (2011).

(2) Determination of the temporal continuity of drought clusters. The temporal connection of drought clusters between adjacent months is determined based on the criterion of their overlap area in space. The drought clusters in adjacent months are regarded as belonging to one event if their overlap area is over 0 km^2, similar to that in Herrera-Estrada et al. (2017). In this way, the splitting or merging activity of drought clusters could be recorded during the drought propagation process.

3.2. Drought characterization

To have a comprehensive understanding of the spatio-temporal variations of droughts in 3-D space–time domain, the following drought characteristics are considered.

(1) Drought duration. It is the time interval from the beginning to the ending of one drought event. In the 3-dimentional structure of one drought event, drought duration is defined as the time length between the initial and the terminal time of the drought space.

(2) Drought area. It is defined as the total area affected by one drought event. It is the projected area over the latitude-longitude surface in the 3-D space–time domain.

(3) Drought severity (S). It indicates the degree of soil water deficit, which is represented by a cumulative value of the 3-SMAPI over total grid pixels within the 3-D space–time domain. Besides, the grid based mean value of 3-SMAPI for the drought events at each month is defined as the drought intensity ($I(t)$). The calculation for drought severity and intensity is as follows:

$$S = \sum_{t=1}^{D} \sum_{j=1}^{n} I_j(t) \tag{1}$$

$$I(\mathrm{t}) = \frac{1}{n} \sum_{j=1}^{n} I_j(t) \tag{2}$$

where $I_j(t)$ indicates the drought intensity of jth grid for all drought clusters at month t in one event, which is the corresponding value of 3-SMAPI on jth grid pixels; n is the total grid number for the drought clusters at month t in one event, D is the drought duration for one event.

(4) Drought tracking characteristics. Drought events are tracked through time by searching for the overlapping grid pixels between temporal adjacent drought clusters in the 3-D drought event identification approach. Similar to such previous studies as Xu et al.(2015), Herrera-Estrada et al. (2017) and Guo et al. (2018), here the spatial changes of a drought over time are represented by the changes of the drought cluster centroids (i.e. the weighted center of 3-SMAPI with 3-SMAPI value at each grid pixel within the drought cluster as weights). During the drought development process, the cluster centroids generate tracks as the drought displace from one to the next month, which is defined as the drought cluster trajectory. In one drought event, one or several drought cluster trajectories might appear due to the merging or splitting activity of the drought cluster.

The monthly displacement of the drought cluster centroid is characterized by the distance and direction of two adjacent cluster centroids

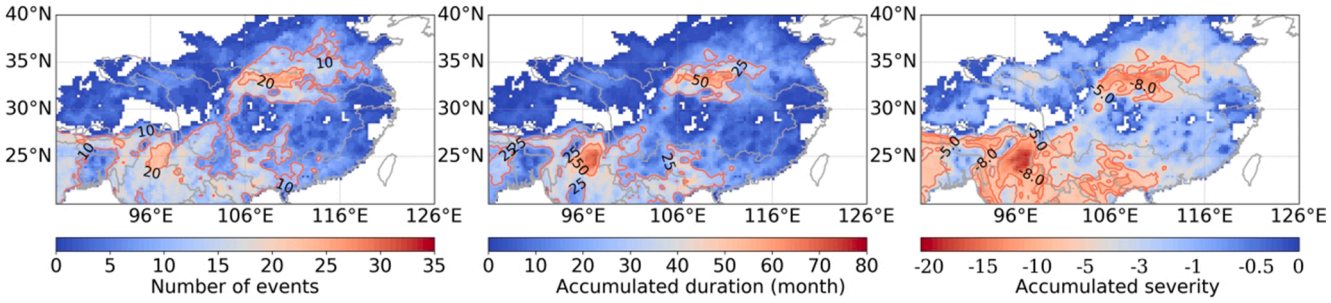

Fig. 2. Spatial distribution of the number of droughts, and the accumulated duration and severity based on the identified drought events over 1979–2016 in a 3-dimentisonal perspective.

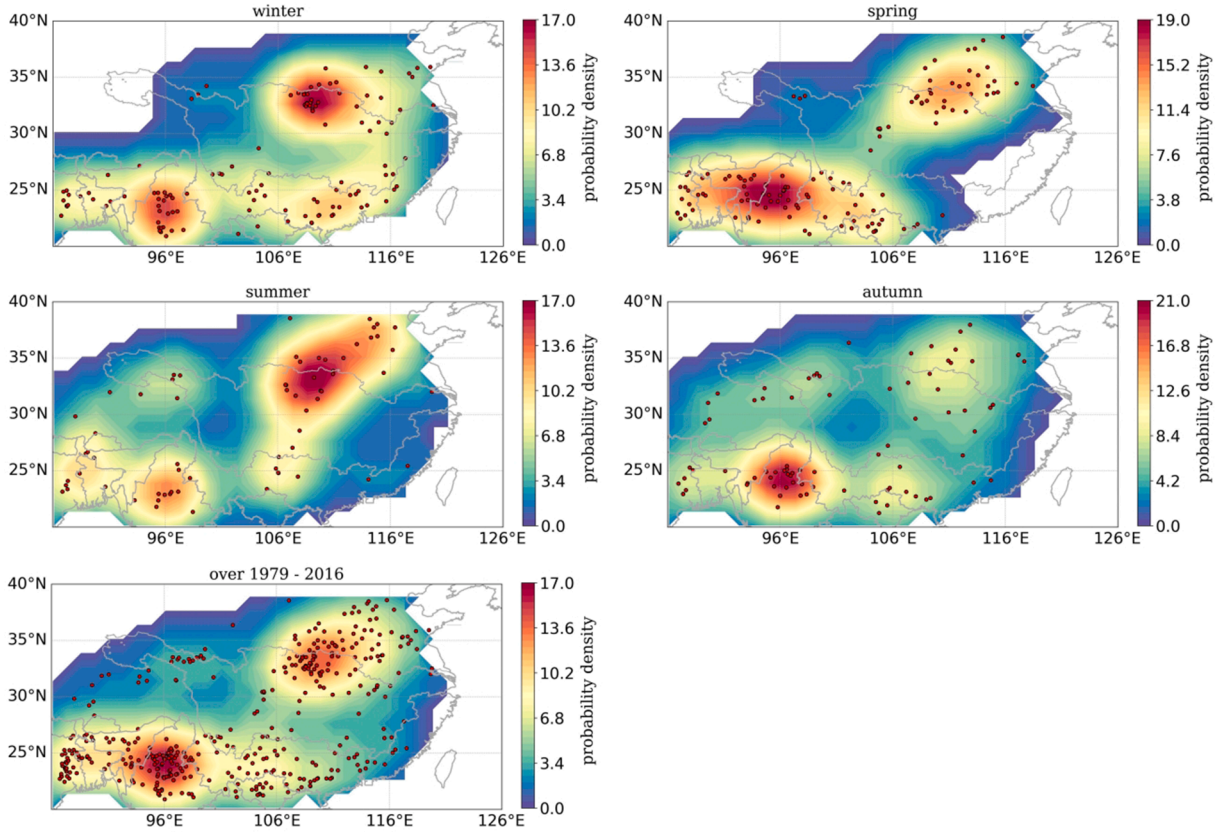

Fig. 3. Spatial distribution of the drought cluster centroids (represented by the red dots) in each season and the total period of 1979–2016 together with their probability density. Note: winter is from December to next February; spring is from March to May; summer is from June to August; autumn is from September to November. (For interpretation of the references to colour in this figure legend, the reader is referred to the web version of this article.)

in time. The total tracking distance of the drought cluster is the cumulative value of the centroid moving distance between adjacent time steps over the whole time span of its tracking process. It indicates the extent and speed of the drought propagation. The direction definition for monthly displacement of drought cluster is referenced from Konapala and Mishra. (2017) and Diaz et al. (2020), which is based on the angle (θ) between the horizontal axis and the line connecting the current and subsequent centroid. Specially, when θ falls in [0°, 22.5°)∪(337.5°, 360°], it indicates the cluster tracking to eastward, θ in [22.5°, 67.5°) indicates northeast, θ in [67.5°, 112.5°) indicates northward, θ in [112.5°, 157.5°) indicates northwest, θ in [157.5°, 202.5°) indicates westward, θ in [202.5°, 247.5°) indicates southwest, θ in [247.5°, 292.5°) indicates southward, and θ in [292.5°, 337.5°) indicates southeast.

4. Results

4.1. Spatial distribution of soil moisture droughts

Based on the 3-D drought identification approach, a total of 369 drought clusters and 145 drought events were identified over the region (Fig. 1(b)) during 1979–2016. Fig. 2 gives an overview of the spatial distribution of SM droughts in terms of their frequency (indicated by the total number of drought events) and the accumulated drought duration and severity. It can be found that the above three drought characteristic parameters present similar spatial pattern. The northeast and southwest of the region experienced comparatively high frequency (>10 events), long duration (>25 months), and more severe (<-5, the smaller negative value represents the more severe droughts) of SM droughts in last four decades. Moreover, northern Myanmar and the upper reach of Han River basin (the largest tributary of Yangtze River) endured the most severe

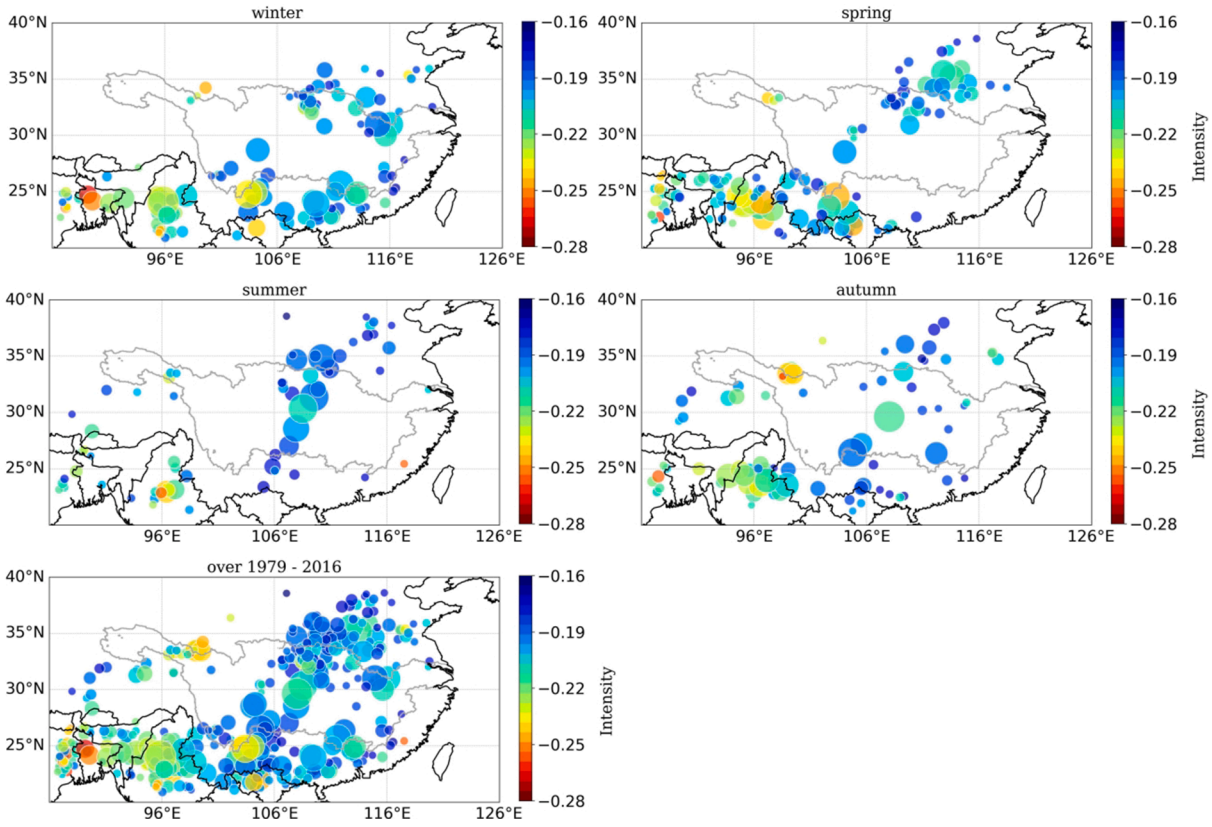

Fig. 4. Maps of the drought cluster (represented by the circle) in each season and the total period of 1979–2016, together with their area (characterized by the circle size) and intensity.

drought condition as the number of drought events > 20, the accumulated drought duration > 50 months and the accumulated drought severity based on 3-SMAPI < -8.

To know the specific spatial distribution of the identified droughts occurred during 1979–2016, the drought cluster centroids (represent the drought cluster's location) together with their probability density are present in Fig. 3, both for the total period and for all four seasons. Generally, the highest probability density (i.e. more cluster centriods) distributes in southwest and northeast of the region, especially for northern Myanmar and the upper reach of Han River basin. This is consistent with that denoted by the accumulated drought characteristic parameters (Fig. 2). In addition, the drought cluster's distribution presents seasonal variations. In winter, it mainly distributes in northeast and southwest of the region, as well as south China. In spring, the drought in southwest spreads out to west and east, and that in northeast stretches along northeast and southwest. However, the drought in southwest becomes less frequent in summer, while that in northeast turns out to be more frequent. In autumn, the drought in southwest seems comeback again.

In addition to drought location, the area and intensity of the identified drought clusters are shown in Fig. 4. Clearly, the drought clusters vary considerably in their area and intensity. The area ranges from 100 to 1667 grids (~625 km^2 per grid) and the intensity (i.e. the area average 3-SMAPI value) from −0.266 to −0.162. Most drought clusters present moderate scale drought as their intensity falls in the range of −0.25 ~ −0.15. The severe drought cluster mainly distributes in southwest, which is applicable for all four seasons. In terms of the occurrence frequency of the drought cluster, the SM drought is more frequent in winter (123 clusters) and spring (125 clusters) than that in summer (66 clusters) and autumn (82 clusters) (for the monthly information see Figure S2 (a)). Moreover, the drought area and severity show comparatively larger value in winter and spring (the cold season) than that in summer and autumn (the warm season) (Figure S2 (b) and (c)). It suggests that SM drought is more serious in cold season than warm season over the region.

4.2. Temporal variation of drought characteristics

On an inter-annual scale, the soil moisture drought of the whole region does not have any significant ($p < 0.05$) trends in terms of the number of drought cluster, the drought area and severity, although large yearly changes presents (Figure S3). However, the seasonal statistics display significant trends. Fig. 5 plots the number of SM drought cluster, and the drought area and severity in each season. In winter, the drought magnitude (indicated by the number of drought cluster and drought area) and severity display slight enhancing trend ($p > 0.05$). Furthermore, the enhancing trend becomes significant in spring as both the number of drought cluster, drought area and severity increased significantly ($p < 0.05$) over time (here the decreasing trend of the actual value of drought severity based on 3-SMAPI represents the increasing drought severity). However, in summer and autumn, the SM drought presents more obvious weakening trend as the drought magnitude and severity decrease significantly ($p < 0.05$). Overall, the SM drought over Southeastern Asia aggravated in cold season (winter and spring), but alleviated in warm season (summer and autumn). To explore the causes behind, the corresponding changes of SM closely related hydrological variable, i.e. precipitation, potential evapotranspiration (PET) and evapotranspiration (ET) in each season are investigated (Fig. 6). In winter, both precipitation and PET exhibit none significant ($p > 0.05$) trend, while ET show significant ($p < 0.05$) increasing trend. The drying trend of SM might be impacted by the increasing PET and ET, as the increasing capacity of ET would extract more moisture from soil and aggravate the SM drought. In spring, the precipitation displays slight decreasing trend while the PET and ET increase significantly ($p < 0.05$).

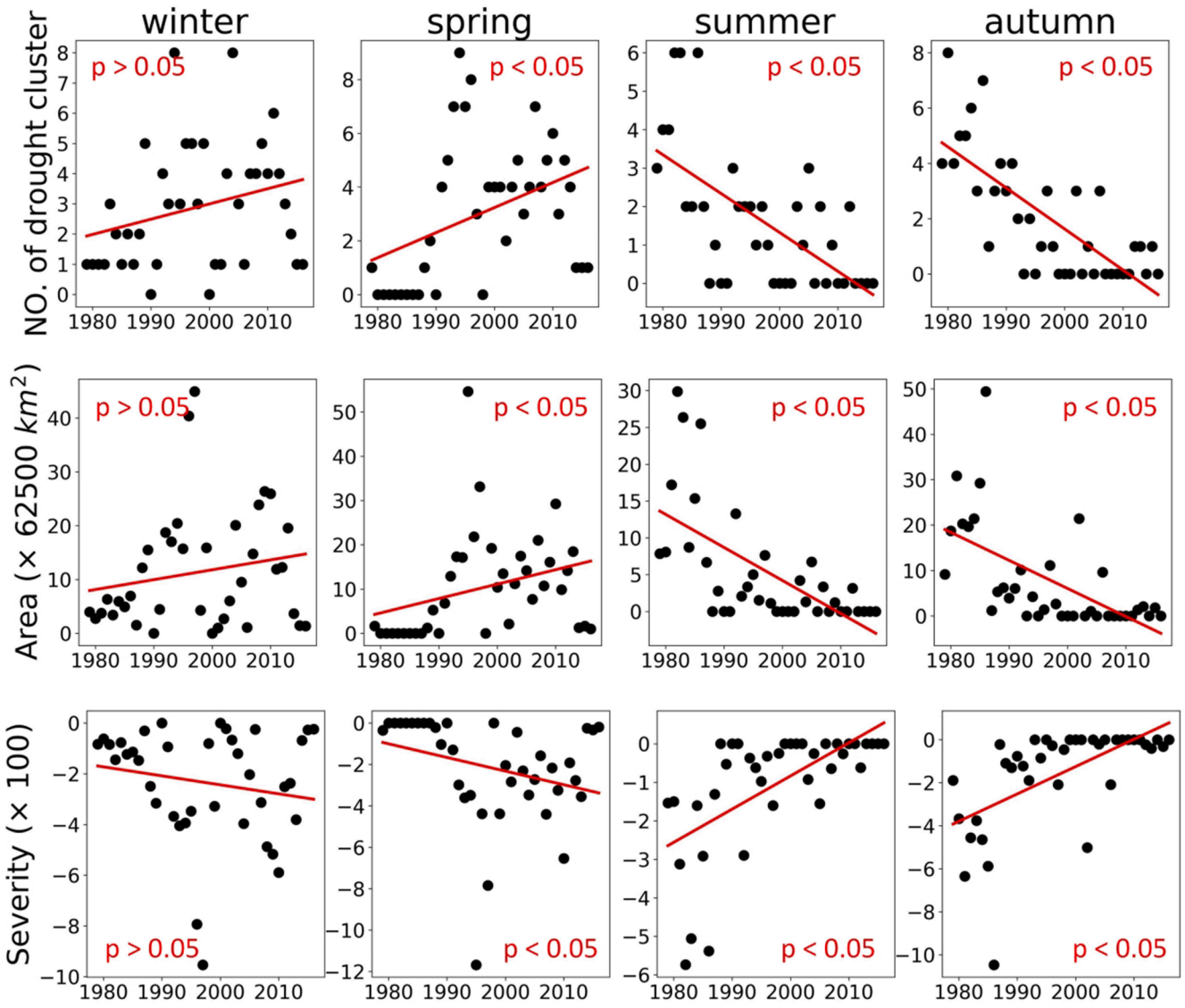

Fig. 5. Trends of the number (NO.) of soil moisture drought cluster, drought area and drought severity for each season.

The significant drying trend of SM should probably be jointly influenced by the decreasing precipitation and the increasing PET, as ET is increased significantly in this case. In summer and autumn, the precipitation presents slight increasing trend while the PET and ET increase significantly ($p < 0.05$). The wetting trend of SM might be related to the increasing precipitation. Although the increasing trend of precipitation is not significant, it is much larger than ET in the magnitude during warm season (see Figure S4).

4.3. Patterns of soil moisture drought trajectory

Among total 145 drought events identified in the framework of the 3-D approach, 90 droughts lasted more than two months, which formed 126 drought cluster trajectories during the drought propagating process in space. Fig. 7 presents the cluster trajectories, together with their cumulative 3-SMAPI value for the drought events started in each season. To avoid spurious large changes of the cluster centroid's location due to its splitting or merging, the cluster tracking with the largest overlap area between the current and subsequent cluster is accounted. Besides, only the tracks with monthly displacements exceeds 150 km are considered lest that the small displacements might fall within the uncertainty of the cluster centroid's location (Herrera-Estrada et al., 2017). It can be seen from Fig. 7 that the cluster tracks and the integrated intensity (the cumulative 3-SMAPI) of the events started in winter, spring, summer and autumn exhibit substantial difference in their spatial patterns. For winter droughts (i.e. the drought events started in winter and mostly lasted in winter and spring), both northeast and south of the study region are active zone (Fig. 7(a)). A predominant route of westward can be found in the cluster tracks located in south region. It can be supported by the direction statistics in Fig. 8 (a), as the westward monthly displacements of the clusters takes up to 34% for winter droughts. However, for summer droughts (i.e. the droughts started in summer and mostly lasting in summer and autumn), the cluster tracks are no longer confined to northeast or southwest region. A predominant route of southwest across Yangtze River basin formed. The cluster tracks toward southwest exceed over 43% of total tracks (Fig. 8 (a)). As for spring droughts, the cluster displacements mostly take place in southwest and northeast region, while no evident routes or directions are present (Fig. 7(b), Fig. 8 (a)). For autumn droughts, the southwest region is the most severe in terms of the integrated intensity. Any dominant tracking route or direction can hardly be found, as the drought cluster tracks scattered in large parts (Fig. 7(d), Fig. 8 (a)). Regarding to the drought cluster tracking distance, the seasonal statistics show that spring droughts have the shortest cluster trajectory on average, while summer droughts usually have

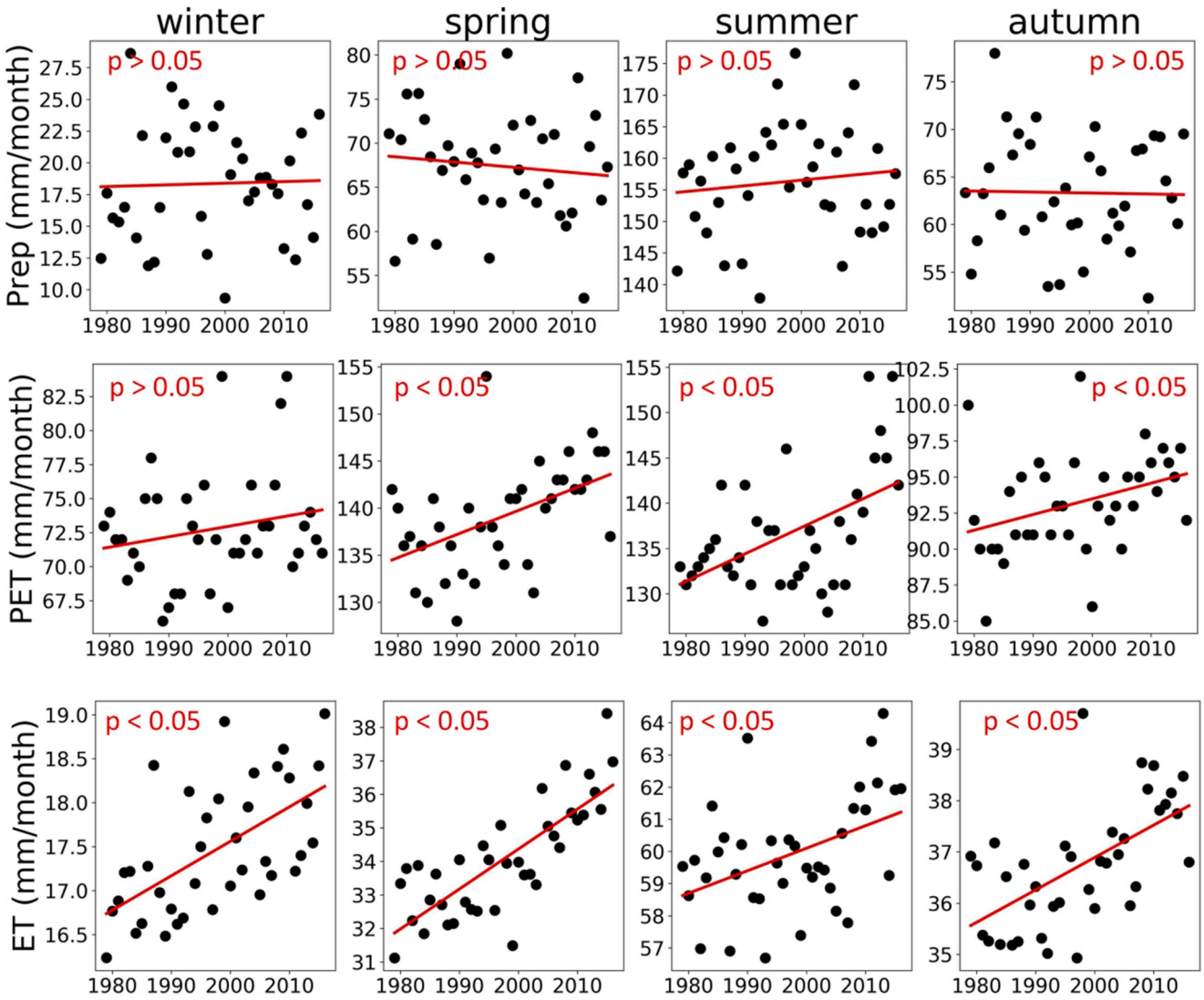

Fig. 6. Trends of precipitation (Prep), potential evapotranspiration (PET) and evapotranspiration (ET) for each season.

longer trajectories (Fig. 8(b)).

4.4. Spatio-temporal developing process of individual drought events

To have an insight into the development process of an individual drought event, the spatio-temporal propagating process of a drought is present explicitly in a 3-dimensional form as Fig. 9. In specific, Fig. 9 shows the drought cluster together with its dynamic monthly displacements of four representative severe events started in winter (Drought Event 200412–200507), spring (Drought Event 199503–199506), summer (Drought Event 198507–198601) and autumn (Drought Event 199611–199706) with different spatial locations. Moreover, the monthly anomaly of two predominant SM controlling factor, i.e. precipitation (the dominant SM input) and potential evapotranspiration (PET, the dominant driver of SM output), in hydrological cycle are also investigated over the 3-D drought affected area to illustrate the possible causes of SM drought. Considering the time lag of precipitation and PET on soil moisture drought (Van Loon and Van Lanen, 2012), the precipitation and PET monthly anomaly maps were accounted and observed 3 months earlier before the drought occurrence (Fig. 10).

The drought event 200412–200507 started in early winter in south China and migrated westward all the way to northern Myanmar over 8 months of duration, although during which the drought cluster splitting and merging phenomenon appeared (Fig. 9 (a)). The initial soil moisture drought was driven by persistent negative abnormal precipitation combined with comparatively strong PET capacity. Meanwhile, the continuation of this drought was probably dominated by precipitation, as its negative anomaly always existed in the drought area and presented a westward change over time (Fig. 10 (a) and (e)). The positive PET anomaly aggravated the SM drought condition to a certain extent as it also presented westward changes during the drought propagation process (Fig. 10 (e)).

The drought event 199503–199506 started in early spring and did not disappear until midsummer. The location of this drought did not change a lot (Figure S5). The occurrence of SM drought in March was resulted from the comparatively low precipitation since January, coupled with the strong PET capacity since February due to crop growing. Likewise, the drought persistence in spring and early summer were under the control of precipitation and PET synergistically, as the negative precipitation anomaly distributed over the whole drought area and the positive PET anomaly presented similar patterns with SM drought cluster (Fig. 10 (b) and (f)).

The drought event 198507–198601 started in midsummer in the middle part of Yangtze River basin with two SM drought cluster appeared simultaneously in the north and south. It travelled to southwest in summer and stranded in southwestern region over 5 months

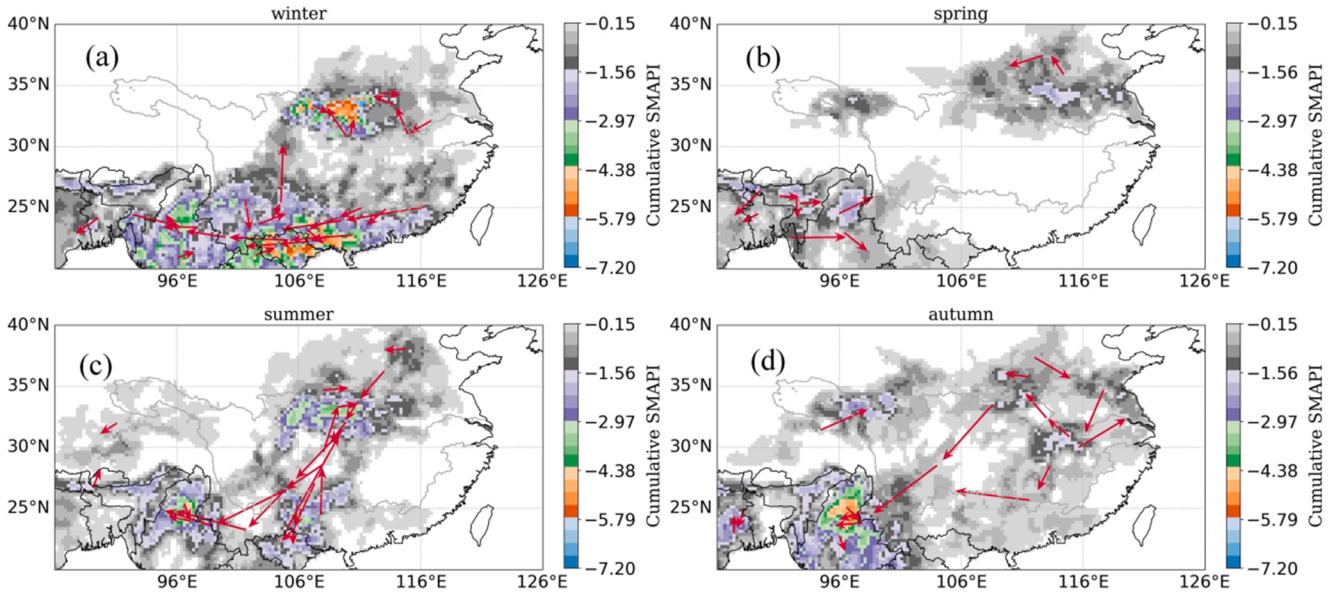

Fig. 7. Drought cluster trajectories (the red arrows) together with their cumulative 3-SMAPI for the drought events started in winter (a), spring (b), summer (c) and autumn (d). Note: only the long tracks (>150 km) are shown. (For interpretation of the references to colour in this figure legend, the reader is referred to the web version of this article.)

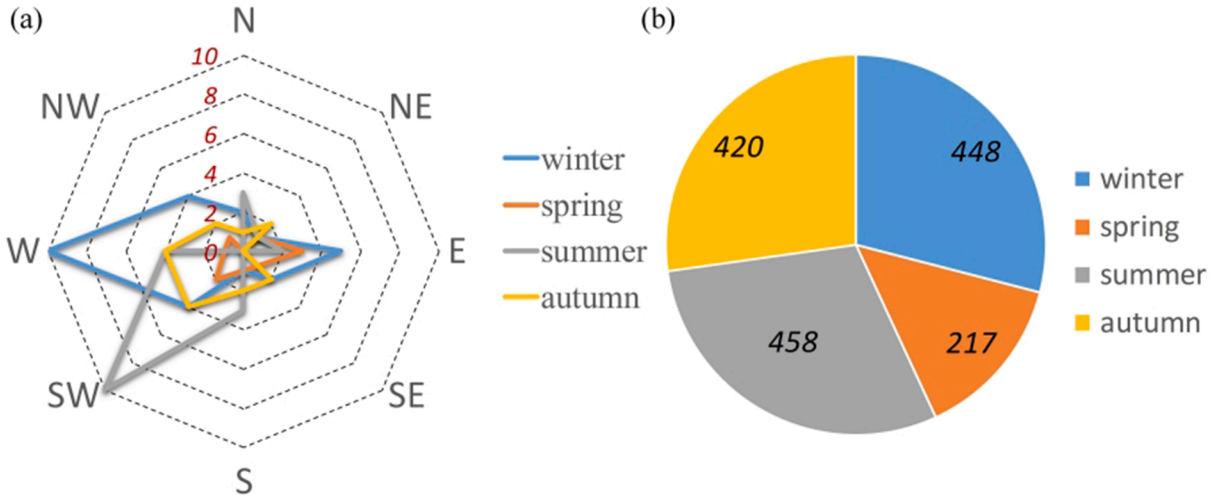

Fig. 8. Direction statistics of the drought cluster tracks (>150 km) (a), and the average distance (km) of drought cluster trajectories (b) for events started in winter, spring, summer and autumn. N, NE, E, SE, S, SW, W, NW are abbreviated for northward, northeast, eastward, southeast, southward, southwest, westward and northwest respectively. 0 ~ 10 indicates the number of drought cluster tracks.

during autumn and winter. The formulation and persistence of this drought is mainly driven by precipitation, because the negative precipitation anomaly nearly filled the whole 3-D drought space. However, the impact of PET cannot be ignored, particularly for SM droughts located in the middle part of Yangtze River basin during summer. It seems that the positive PET anomaly in summer contributed the appearance of SM drought, while the negative PET anomaly after summer promoted its disappearance (Fig. 10 (c) and (g)).

The drought event 199611–199706 started in late autumn in southwest of Yangtze River basin (mainly in Yunnan province, China), stranded in southwest of the region over the whole winter and spring and finally disappeared as summer came. The drought occurrence firstly in Yunnan province should be driven by precipitation and PET, as where the two drivers both present anomaly from August to November (Fig. 10 (d) and (h)). Additionally, the precipitation and PET monthly anomaly map also indicated that the southwest drought in winter was probably dominated by precipitation anomaly, while the drought in spring should largely rely on the PET anomaly. This change can be related to the temperature increase and the crop growing in spring.

Overall, the above spatio-temporal development process of SM droughts, and the precipitation and PET in drought space–time structure indicated that SM drought propagated synergistically with precipitation and PET. Precipitation was generally the primary driver and PET the secondary, particularly for the drought events lasting in summer and winter in south region. Nevertheless, PET usually enhanced the SM drought condition in spring and summer due to the temperature increasing and the crop growing vigorously.

5. Discussion

5.1. Robustness of the identified predominant route of drought

Two predominant routes of westward for winter droughts in south region and southwest for summer droughts across Yangtze River basin

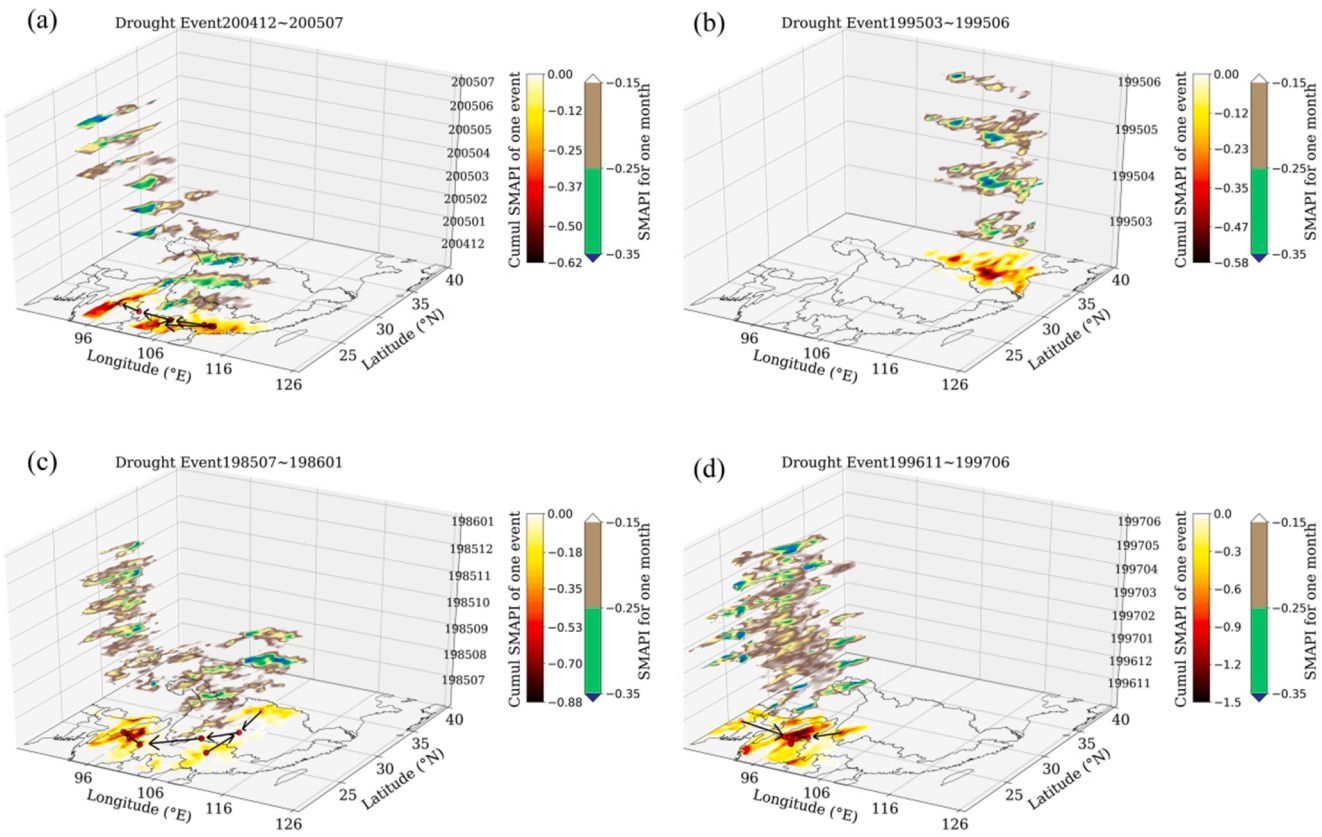

Fig. 9. Spatio-temporal propagation process of four severe representative events started in winter (a), spring (b), summer (c) and autumn (d) with different spatial locations. The red dots are the drought cluster centroids and the black arrows represent the cluster displacement tracks. Note: the drought cluster tracks are not clear for (b) due to the quite small changes of the cluster centroids and the 3-dimensional projection. The clear tracks are present in a 2-dimensional map (Figure S5). (For interpretation of the references to colour in this figure legend, the reader is referred to the web version of this article.)

from northeast to southwest of the region are recognized, based on the 0.25°×0.25° ESA CCI soil moisture data using SMAPI on 3-month scale (Fig. 7(a) and (c)). For seasonal (3 monthly SMAPI) soil moisture droughts, the two predominant drought cluster tracking routes are ubiquitous or just specific for the 0.25° spatial resolution? Considering the fact that the specific information of soil moisture tends to disappear, while the primary one usually remains with the declining of its spatial resolution owing to space averaging, the drought tracking characteristics were investigated based on the coarse (0.5°×0.5° and 1.0°×1.0°) spatial data. Both the 0.5°×0.5° and 1.0°×1.0° soil moisture data are resampled from the original 0.25°×0.25° ESA CCI dataset using a spatial averaging method.

Fig. 11 shows the drought cluster trajectories together with their cumulative 3-SMAPI for the drought events started in winter and summer for both 0.5°×0.5° and 1.0°×1.0° cases. It can be found that the spatial distribution and direction of the cluster tracks have certain changes among different spatial resolutions both for winter and summer droughts (Fig. 7 (a) and (c), Fig. 11 (a) and (b), Fig. 11 (c) and (d)). However, both the westward predominant route for winter droughts and the southwest route for summer droughts still exists in the cases with lower spatial resolution. It is also supported by the direction statistics of the drought cluster tracks (Fig. 12). For winter droughts, the westward monthly displacements of clusters are up to 48% and 39% in 0.5°×0.5° and 1.0°×1.0° cases respectively. For summer droughts, the cluster tracks toward southwest is 38% in 1.0°×1.0° case. Although it is 22% in 0.5°×0.5° case, the total of southward, southwest and westward is up to 70%. Overall, the existence of the predominant route of westward for winter droughts in south region and southwest route for summer droughts across Yangtze River basin should be objective.

5.2. Reasonability of the predominant route of drought

Droughts can span over large geographical areas and last for months. Drought propagation occurs in space and time simultaneously. The underlying causes for drought propagation is still unclear as a significant number of physical processes related to atmospheric activity, land–atmosphere feedback and land surface process are involved in it. To date, two primary mechanisms of precipitation recycling and moisture transport have been linked to soil moisture drought propagation (Roy et al., 2019; Miralles et al., 2019). Precipitation recycling is from regional moisture recycling perspective, mainly refers to the contribution of evapotranspiration (ET) from a region to the precipitation of the same region in drought development (Eltahir and Bras, 1996). Moisture transport focuses on the horizontal movement of water vapor, which is interpreted as a process that drought reduce moisture exports downwind, leading to less precipitation and possibly amplify the drought condition downwind in Herrera-Estrada et al. (2019). Precipitation recycling is from the perspective of the impact of regional internal moisture circulation on drought propagation, while moisture transport is from the effect of the decreased/increased moisture from upwind to downwind on drought condition. Actually, both the precipitation recycling and moisture transport mechanism are likely to co-exist in soil moisture drought propagation. In the above two mechanisms, soil moisture drought propagation is inseparable with the primary controlling factor of SM, i.e. precipitation (Prep, the dominant SM input) and potential evapotranspiration (PET, the dominant driver of SM output). At a certain level, PET/Prep (precipitation) could reflect the drying capacity/potential of SM, with the larger value indicates the more likely dryer of SM. Besides, considering that PET affects SM variations through the actual ET of the land surface soil and vegetation, ET should also be

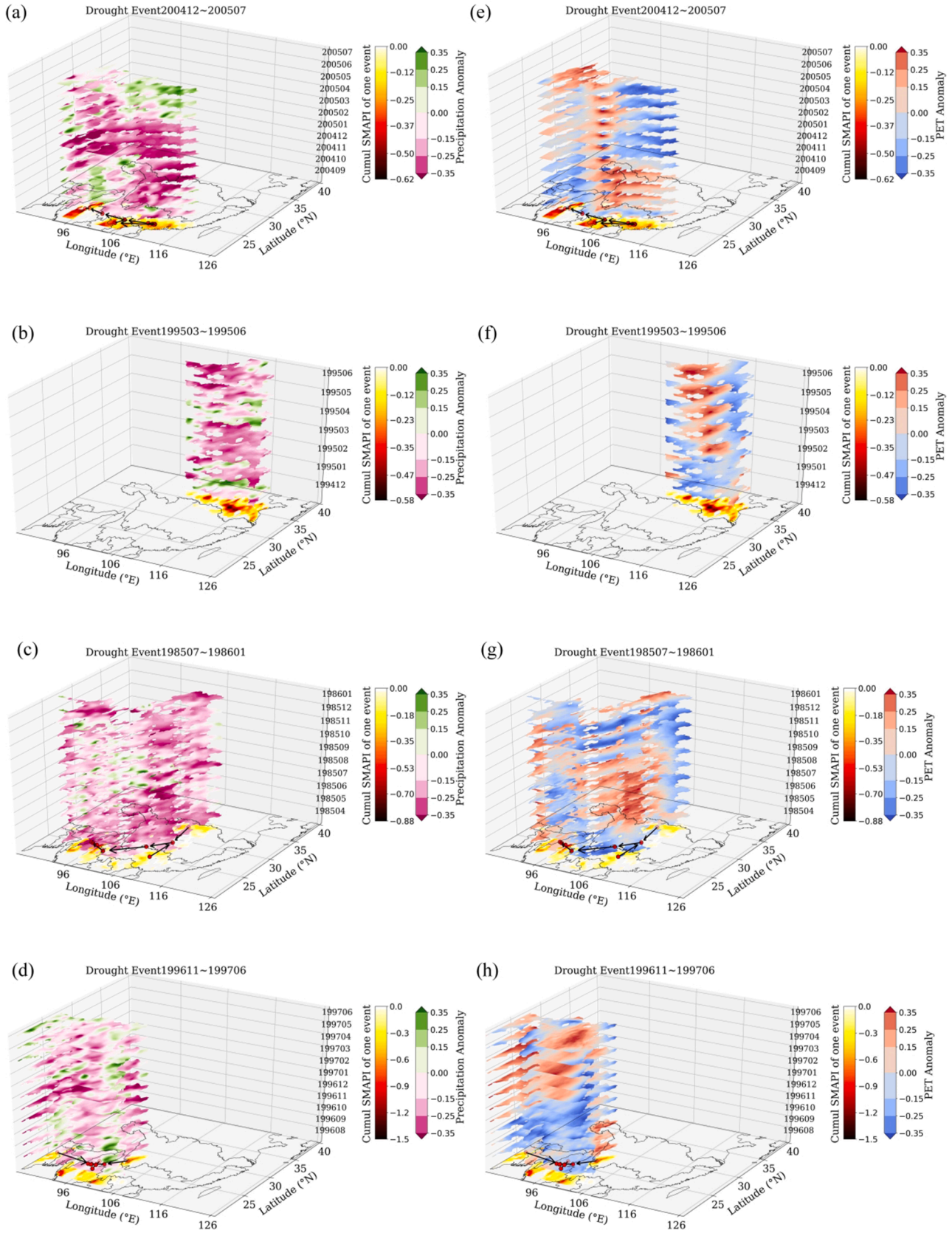

Fig. 10. Monthly anomaly maps of precipitation and potential evapotranspiration (PET) before (3 months) and within the soil moisture drought duration over the drought affected area for event 200412–200507 (a) (e), 199503–199506 (b) (f), 198507–198601 (c) (g) and 199611–199706 (d) (h). Note: the bottom layer shows the soil moisture drought cluster tracks and their cumulative SMAPI value in one event (the same to Fig. 9).

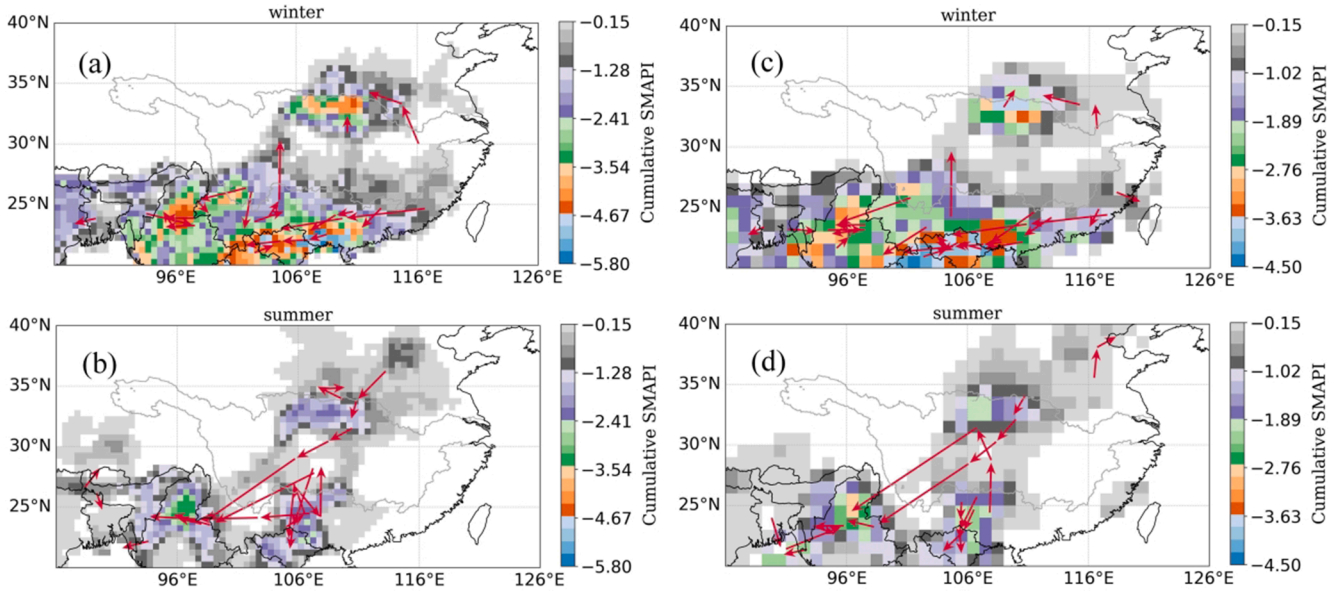

Fig. 11. Drought cluster trajectories (the red arrows) together with their cumulative 3-SMAPI for the drought events started in winter and summer. (a) and (b) is based on the 0.5°×0.5° soil moisture resampled from the original 0.25°×0.25° data, while (c) and (d) is based on the 1.0°×1.0° resampled data. Note: only the long tracks (>150 km) are shown. (For interpretation of the references to colour in this figure legend, the reader is referred to the web version of this article.)

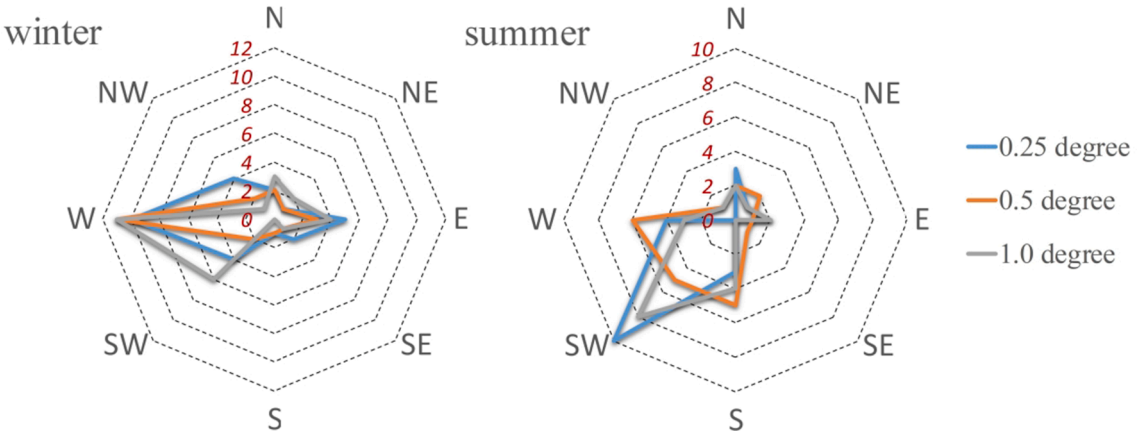

Fig. 12. Direction statistics of the drought cluster tracks (>150 km) for events started in winter and summer in three cases of 0.25°×0.25°, 0.5°×0.5° and 1.0°×1.0°. N, NE, E, SE, S, SW, W, NW are abbreviated for northward, northeast, eastward, southeast, southward, southwest, westward and northwest respectively. 0 ~ 12/10 indicates the number of drought cluster tracks.

accounted as a prerequisite in SM drought propagation exploration. Hence, we try to elaborate the reasonability of the identified predominant routes in our drought cluster tracking by analyzing the monthly variation of PET/P and ET combing the drought development mechanism of precipitation recycling and moisture transport.

The westward predominant route in droughts started in winter and lasting in winter half year (winter and spring) in south of the region can be interpreted as follows. In winter and spring, the actual ET in south (especially for southwest) is still at relatively high level (Fig. 14), because the temperature generally keeps above 10 centigrade with subtropical climate, and both the vegetation growing and soil/water bodies evaporation needs plenty of water supply. Under this condition, the low abnormal Prep combined with relatively high capacity of ET (PET) tends to cause SM drought. In terms of drought propagation, the westward route in south is probably related to the expansion of the high drying capacity of SM (i.e. high PET/Prep) in space over time (the black box, Fig. 13). The westward expansion of dryness is likely related to the following two factors. One is the prevailing easterly winds in winter (mainly for Dec and Jan) in eastern part of the south region and its upwind area (the red box, Figure S6). The easterly winds would drive dry atmosphere westward and amplify the drought condition downwind as it is opposite to the general moisture transport direction of eastward (Ding et al., 2018; Wang and Lin, 2002). The other is the westerly and southwesterly winds in later winter and spring in south of the region (the blue box, Figure S6). The prevailing westerly winds tend to drive moist atmosphere eastward and relieve the drought condition downwind as it is consistent with the general moisture transport direction of eastward (Fang et al., 2013; Ding et al., 2018). Besides, it should be noteworthy that in north region, SM droughts cannot be indicated by the substantially high PET/Prep in winter half year. It is because the actual ET is comparatively low there (Fig. 14, Dec to Mar) due to the limited evaporation from soil/water bodies and the very little transpiration from the stagnant growth of vegetation subjected to the persistent low temperature (subzero in general) in winter and early spring. Correspondingly, the southwest predominant route in droughts started in summer and lasting in summer half year (summer and autumn) across Yangtze River basin can be illustrated below. With the coming of summer, the evaporation from soil/water bodies increases and the plant grows vigorously

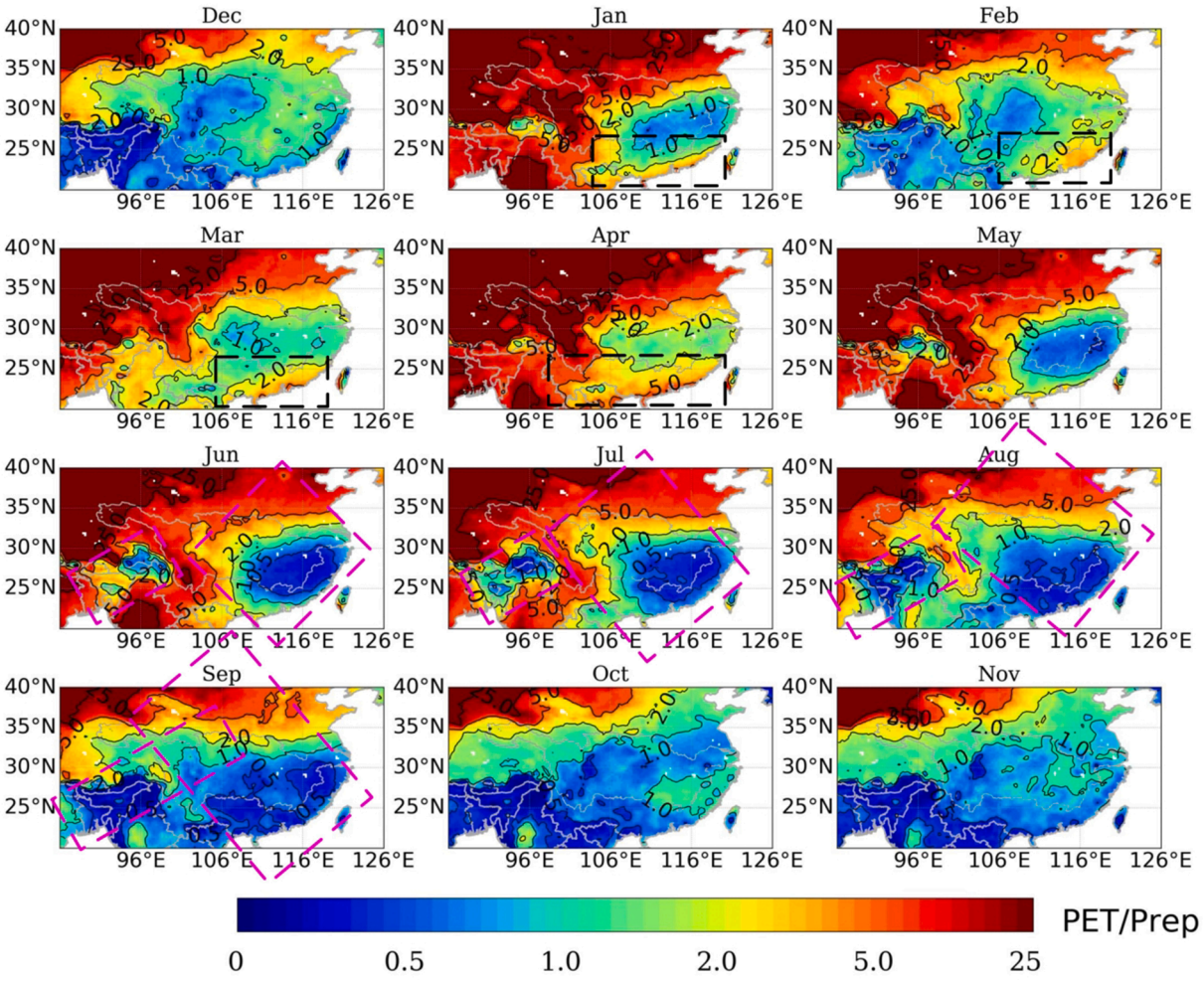

Fig. 13. Monthly average value of PET/Prep over 1979–2016. PET and Prep are abbreviated for Potential evapotranspiration and Precipitation respectively. Note: Dec, Jan, Feb, Mar, Apr, Jun, Jul, Aug, Sep, Oct and Nov are abbreviated for December, January, February, March, April, June, July, August, September, October and November respectively.

and demands large amounts of water for transpiration over most of the region (Fig. 14). The PET is usually high, while the Prep is often unevenly distributed in space and time caused by the seasonal northward advance and southward retreat of the rain belt (Ding and Chan, 2005). This contradiction between water demand and supply increases the probability of drought. The monthly climatology shows that the low drying capacity of SM (i.e. the low PET/Prep) expands toward northeast and northwest (the magenta box, Fig. 13), which is largely impacted by the water vapor transport via the southwest monsoon from Indian Ocean and the southeast monsoon from Pacific Ocean (Jun to Nov, Figure S6). Based on the moisture transport mechanism, the drought should propagate to the opposite direction (i.e. southwest/southeast) with the low PET/Prep (i.e. high level of moisture) expansion. Probably, because the drought over northeast-southwest of the region is mainly impacted by the water vapor transport from southwest in summer half year, the SM drought propagation presents a southwest predominant tracking route.

6. Conclusion

To deepen the understanding of drought propagation in multiple dimensions for further drought mechanism exploration and effective drought prediction, the soil moisture droughts in a hotspot region of Southeastern Asia were investigated based on a 3-dimensional (latitude, longitude and time) drought identification approach with a merged dataset of remote sensing and land surface modeling over 1979–2016. The results demonstrated that:

(i) A total of 369 drought clusters and 145 drought events were identified based on 3-SMAPI. Spatially, severe droughts mainly distributed in southwest and northeast of the study region. The SM drought was more serious in cold season (winter and spring) than that in warm season (summer and autumn) in terms of the frequency, area and severity of the drought cluster.

(ii) Although the SM drought for the whole region did not show any distinct trend on an inter-annual scale, it presented significant ($p < 0.05$) trend on seasonal scale. The drought in warm season alleviated, but that in cold season aggravated prominently. Thus, it would pose more challenges for future drought mitigation in cold season, especially for spring with crop growing vigorously.

(iii) In drought cluster tracking, two predominant routes of westward and southwest were recognized. The westward route was shared by the droughts started in winter and lasted mainly in winter half year in south region, while the southwest route was shared by the droughts started in summer and lasted mainly in summer half year across Yangtze River basin from northeast to southwest of the region.

(iv) At an event level, SM drought propagated synergistically with precipitation and potential evapotranspiration (PET). Generally, precipitation was the primary driver and PET the secondary, particularly for the droughts lasting in summer and winter in

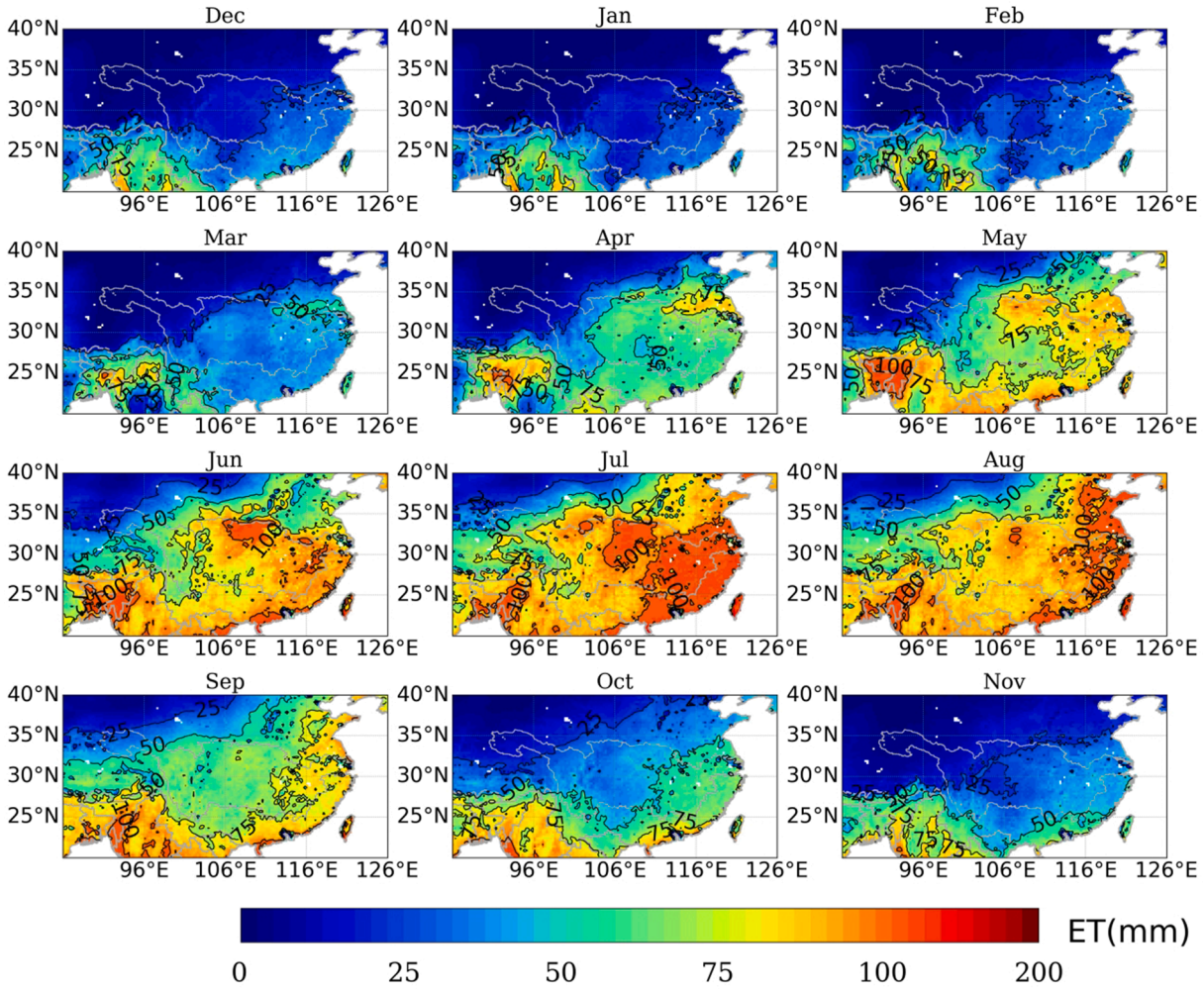

Fig. 14. Monthly average value of Evapotranspiration (ET) over 1979–2016.

south region. Nevertheless, the driving power of PET usually enhanced in spring and summer with the temperature increasing and the crop growing vigorously.

Overall, the current work gave a comprehensive investigation on the spatio-temporal dynamics and characteristics of soil moisture droughts in a global hotspot region of Southeastern Asia with typical monsoon climate. The existence of the predominant drought tracking route for seasonal SM droughts was largely confirmed based on the categorical analysis of season/timing of drought. The innovative drought tracking analysis could serve as important implications for investigation on drought migration patterns of other hotspot regions with monsoon climate. The dynamics of SM droughts in the 3-D drought domain was interpreted in consideration of the dominant SM input (precipitation) and output (PET). The findings in drought propagation is the foundation to understand the driver on drought development, which would also provide essential spatio-temporal structure for further drought mechanism exploration and important clues for future drought prediction.

CRediT authorship contribution statement

Yongwei Liu: Conceptualization, Data curation, Formal analysis, Funding acquisition, Investigation, Methodology, Validation, Visualization, Writing - original draft, Writing - review & editing. **Yuanbo Liu:** Conceptualization, Project administration, Supervision. **Wen Wang:** Resources, Writing - review & editing, Supervision. **Han Zhou:** Methodology, Writing - review & editing.

Declaration of Competing Interest

The authors declare that they have no known competing financial interests or personal relationships that could have appeared to influence the work reported in this paper.

Acknowledgments

This work was supported by the National Natural Science Foundation of China (41901049, 41430855, 41971042), Jiangsu Science and Technology Planning Youth Project (BK20191097) and National key Research and development program (2018YFE0105900).

Appendix A. Supplementary data

Supplementary data to this article can be found online at https://doi.org/10.1016/j.jhydrol.2020.125906.

References

Andreadis, K.M., Clark, E.A., Wood, A.W., Hamlet, A.F., Lettenmaier, D.P., 2005. Twentieth-century drought in the conterminous United States. J. Hydrometeorol. 6 (6), 985–1001. https://doi.org/10.1175/Jhm450.1.

Andreadis, K.M., Lettenmaier, D.P., 2006. Trends in 20th century drought over the continental United States: U.S. DROUGHT TRENDS. Geophys. Res. Lett. 33 (10), n/a–n/a. https://doi.org/10.1029/2006GL025711.

Cattani, E., Merino, A., Levizzani, V., 2016. Evaluation of monthly satellite-derived precipitation products over East Africa. J. Hydrometeorol. 17 (10), 2555–2573. https://doi.org/10.1175/JHM-D-15-0042.1.

Dai, A., 2011. Characteristics and trends in various forms of the Palmer Drought Severity Index during 1900–2008. J. Geophys. Res. 116 (D12) https://doi.org/10.1029/2010JD015541.
Diaz, V., Corzo Perez, G.A., Van Lanen, H.A.J., Solomatine, D., Varouchakis, E.A., 2020. An approach to characterise spatio-temporal drought dynamics. Adv. Water Resour. 137, 103512. https://doi.org/10.1016/j.advwatres.2020.103512.
Ding, Y., Chan, J.C.L., 2005. The East Asian summer monsoon: an overview. Meteorol. and Atmos. Phys. 89(1-4): 117-142. https://doi.org/10.1007/s00703-005-0125-z.
Ding, Y., Si, D., Liu, Y., Wang, Z., Li, Y., Zhao, L., Song, Y., 2018. The characteristics, driving force and interdecadal variation of summer winds in East Asia [In Chinese]. Atmospheric Science 42 (03), 533–558.
Eltahir, E.A.B., Bras, R.L., 1996. Precipitation recycling. Rev. Geophys. 34 (3), 367–378. https://doi.org/10.1029/96RG01927.
Fang, Y., Zhang, Y., Huang, A., Li, B.o., 2013. Seasonal and intraseasonal variations of East Asian summer monsoon precipitation simulated by a regional air-sea coupled model. Adv. Atmos. Sci. 30 (2), 315–329. https://doi.org/10.1007/s00376-012-1241-6.
Fischer, T., Gemmer, M., Lüliu, L., Buda, S.u., 2011. Temperature and precipitation trends and dryness/wetness pattern in the Zhujiang River Basin, South China, 1961–2007. Quat. Int. 244 (2), 138–148. https://doi.org/10.1016/j.quaint.2010.08.010.
Gocic, M., Trajkovic, S., 2014. Spatiotemporal characteristics of drought in Serbia. J. Hydrol. 510, 110–123. https://doi.org/10.1016/j.jhydrol.2013.12.030.
Guo, H., Bao, A., Ndayisaba, F., Liu, T., Jiapaer, G., El-Tantawi, A.M., De Maeyer, P., 2018. Space-time characterization of drought events and their impacts on vegetation in Central Asia. J. Hydrol. 564, 1165–1178. https://doi.org/10.1016/j.jhydrol.2018.07.081.
Konapala, G., Mishra, A., 2017. Review of complex networks application in hydroclimatic extremes with an implementation to characterize spatio-temporal drought propagation in continental USA. J. Hydrol. 555, 600–620. https://doi.org/10.1016/j.jhydrol.2017.10.033.
Hannah, R., Max, R., 2013. Land Use. Published online at OurWorldInData.org. Retrieved from: 'https://ourworldindata.org/land-use' [Online Resource].
Herrera-Estrada, J.E., Satoh, Y., Sheffield, J., 2017. Spatiotemporal dynamics of global drought. Geophys. Res. Lett. 44 (5), 2254–2263. https://doi.org/10.1002/2016GL071768.
Huang, Q., Sun, Z., Opp, C., Lotz, T., Jiang, J., Lai, X., 2014. Hydrological Drought at Dongting Lake: Its Detection, Characterization, and Challenges Associated With Three Gorges Dam in Central Yangtze, China. Water Resour Manage 28 (15), 5377–5388. https://doi.org/10.1007/s11269-014-0807-8.
Lievens, H., De Lannoy, G.J.M., Al Bitar, A., Drusch, M., Dumedah, G., Hendricks Franssen, H.-J., Kerr, Y.H., Tomer, S.K., Martens, B., Merlin, O., Pan, M., Roundy, J. K., Vereecken, H., Walker, J.P., Wood, E.F., Verhoest, N.E.C., Pauwels, V.R.N., 2016. Assimilation of SMOS soil moisture and brightness temperature products into a land surface model. Remote Sens. Environ. 180, 292–304. https://doi.org/10.1016/j.rse.2015.10.033.
Liu, Y., Liu, Y., Wang, W., 2019a. Inter-comparison of satellite-retrieved and Global Land Data Assimilation System-simulated soil moisture datasets for global drought analysis. Remote Sens. Environ. 220, 1–18. https://doi.org/10.1016/j.rse.2018.10.026.
Liu, Y., Zhu, Y., Ren, L., Singh, V. P., Yong, B., Jiang, S., Yang, X., 2019b. Understanding the Spatiotemporal Links Between Meteorological and Hydrological Droughts From a Three-Dimensional Perspective. J. Geophys. Res. Atmos. 124(6), 3090-3109. https://doi.org/10.1029/2018JD028947.
Liu, Y.Y., Parinussa, R.M., Dorigo, W.A., De Jeu, R.A., Wagner, W., Van Dijk, A.I.J.M., Evans, J.P., 2011a. Developing an improved soil moisture dataset by blending passive and active microwave satellite-based retrievals. Hydrol. Earth Syst. Sci. 15 (2), 425. https://doi.org/10.5194/hess-15-425-2011.
Liu, Y.Y., de Jeu, R.A.M., McCabe, M.F., Evans, J.P., van Dijk, A.I.J.M., 2011b. Global long-term passive microwave satellite-based retrievals of vegetation optical depth: long-term vegetation optical depth. Geophys. Res. Lett. 38 (18), n/a–n/a. https://doi.org/10.1029/2011GL048684.
Liu, Z., Wang, Y., Shao, M., Jia, X., Li, X., 2016. Spatiotemporal analysis of multiscalar drought characteristics across the Loess Plateau of China. J. Hydrol. 534, 281–299. https://doi.org/10.1016/j.jhydrol.2016.01.003.
Liu, Y., Wu, G., 2016. Hydroclimatological influences on recently increased droughts in China's largest freshwater lake. Hydrol. Earth Syst. Sci. 20 (1), 93–107. https://doi.org/10.5194/hess-20-93-2016.
Lloyd-Hughes, B., 2012. A spatio-temporal structure-based approach to drought characterisation: a structure-based approach to drought characterisation. Int. J. Climatol. 32 (3), 406–418. https://doi.org/10.1002/joc.2280.
Miralles, D.G., Gentine, P., Seneviratne, S.I., Teuling, A.J., 2019. Land-atmospheric feedbacks during droughts and heatwaves: State of the science and current challenges: Land feedbacks during droughts and heatwaves. Ann. N. Y. Acad. Sci. 1436 (1), 19–35. https://doi.org/10.1111/nyas.13912.
Reichle, R.H., Koster, R.D., 2004. Bias reduction in short records of satellite soil moisture. Geophys. Res. Lett. 31 (19) https://doi.org/10.1029/2004GL020938.
Roy, T., Martinez, J.A., Herrera-Estrada, J.E., Zhang, Y., Dominguez, F., Berg, A., et al., 2019. Role of moisture transport and recycling in characterizing droughts: Perspectives from two recent US droughts and the CFSv2 system. J. Hydrometeorol. 20, 139–154. https://doi.org/10.1175/JHM-D-18-0159.1.
Schneider, U., Finger, P., Meyer-Christoffer, A., Rustemeier, E., Ziese, M., Becker, A., 2017. Evaluating the hydrological cycle over land using the newly-corrected precipitation climatology from the Global Precipitation Climatology Centre (GPCC). Atmosphere 8 (3), 52. https://doi.org/10.3390/atmos8030052.
Sheffield, J., Andreadis, K.M., Wood, E.F., Lettenmaier, D.P., 2009. Global and Continental Drought in the Second Half of the Twentieth Century: Severity-Area-Duration Analysis and Temporal Variability of Large-Scale Events. J. Climate. 22 (8), 1962–1981. https://doi.org/10.1175/2008JCLI2722.1.
Sheffield, J., Wood, E.F., 2008. Global trends and variability in soil moisture and drought characteristics, 1950–2000, from observation-driven simulations of the terrestrial hydrologic cycle. J. Climate. 21 (3), 432–458. https://doi.org/10.1175/2007JCLI1822.1.
Sun, S., Chen, H., Wang, G., Li, J., Mu, M., Yan, G., Xu, B., Huang, J., Wang, J., Zhang, F., Zhu, S., 2016. Shift in potential evapotranspiration and its implications for dryness/wetness over Southwest China: PET shift and its implications. J. Geophys. Res. Atmos. 121 (16), 9342–9355. https://doi.org/10.1002/2016JD025276.
Sun, S., Chen, H., Sun, G., Ju, W., Wang, G., Li, X., Zhu, S., 2017. Attributing the changes in reference evapotranspiration in Southwestern China using a new separation method. J. Hydrometeorol. 18(3), 777-798. https://doi.org/10.1175/JHM-D-16-0118.1.
Van Loon, A., Van Lanen H., 2012. A process-based typology of hydrological drought. Hydrol. Earth Syst. Sci. 16(7): 1915. https://doi.org/10.5194/hess-16-1915-2012.
Vicente-Serrano S.M., Begueria S., Lorenzo-Lacruz J., Camarero, J.J., Lopez-Moreno, J.I., Juan, I., et al., 2012. Performance of drought indices for ecological, agricultural, and hydrological applications. Earth Interact. 16(10):1–27. https://doi.org/10.1175/2012EI000434.1.
Wang, A., Lettenmaier, D.P., Sheffield, J., 2011. Soil moisture drought in China, 1950–2006. J. Climate. 24 (13), 3257–3271. https://doi.org/10.1175/2011JCLI3733.1.
Wang, B., Lin, H., 2002. Rainy season of the Asian-Pacific summer monsoon. J. Climate. 15 (4), 386–398. https://doi.org/10.1175/1520-0442(2002)015<0386:RSOTAP>2.0.CO;2.
Wang, L., Huang, G., Chen, W., Zhou, W., Wang, W., 2018. Wet-to-dry shift over Southwest China in 1994 tied to the warming of tropical warm pool. Clim Dyn 51 (7-8), 3111–3123. https://doi.org/10.1007/s00382-018-4068-8.
Wu, Z., Mao, Y., Li, X., Lu, G., Lin, Q., Xu, H., 2016. Exploring spatiotemporal relationships among meteorological, agricultural, and hydrological droughts in Southwest China. Stoch Environ Res Risk Assess 30 (3), 1033–1044. https://doi.org/10.1007/s00477-015-1080-y.
Xu, K., Yang, D., Yang, H., Li, Z., Qin, Y., Shen, Y., 2015. Spatio-temporal variation of drought in China during 1961–2012: A climatic perspective. J. Hydrol. 526, 253–264. https://doi.org/10.1016/j.jhydrol.2014.09.047.
Yang, P., Xiao, Z., Yang, J., Liu, H., 2013. Characteristics of clustering extreme drought events in China during 1961–2010. Acta Meteorol Sin 27 (2), 186–198. https://doi.org/10.1007/s13351-013-0204-x.
Yuan, X., Ma, Z., Pan, M., Shi, C., 2015. Microwave remote sensing of short-term droughts during crop growing seasons. Geophys. Res. Lett. 42 (11), 4394–4401. https://doi.org/10.1002/2015GL064125.
Zhai, J., Huang, J., Su, B., Cao, L., Wang, Y., Jiang, T., Fischer, T., 2017. Intensity–area–duration analysis of droughts in China 1960–2013. Clim. Dyn. 48 (1-2), 151–168. https://doi.org/10.1007/s00382-016-3066-y.
Zhan, W., Guan, K., Sheffield, J., Wood, E.F., 2016. Depiction of drought over sub-Saharan Africa using reanalyses precipitation data sets: Depiction of Drought Using Reanalyses. J. Geophys. Res. Atmos. 121 (18), 10,555–10,574. https://doi.org/10.1002/2016JD024858.
Zhang, Q.i., Ye, X.-C., Werner, A.D., Li, Y.-L., Yao, J., Li, X.-h., Xu, C.-y., 2014. An investigation of enhanced recessions in Poyang Lake: Comparison of Yangtze River and local catchment impacts. J. Hydrol. 517, 425–434. https://doi.org/10.1016/j.jhydrol.2014.05.051.
Zhang X., Tang Q., Liu X., et al., 2017. Soil moisture drought monitoring and forecasting using satellite and climate model data over Southwestern China. J. Hydrometeorol. 18(1): 5-23. https://doi.org/10.1175/JHM-D-16-0045.1.
Zhou, H., Liu, Y., 2018. Spatio-temporal pattern of meteorological droughts and its possible linkage with climate variability: spatio-temporal pattern of meteorological droughts. Int. J. Climatol 38 (4), 2082–2096. https://doi.org/10.1002/joc.5319.
Zhou, H., Liu, Y., Liu, Y., 2019. An approach to tracking meteorological drought migration. Water Resour. Res. 55 (4), 3266–3284. https://doi.org/10.1029/2018WR023311.